AN INVESTIGATION INTO THE ORIGIN OF THE CARBUNCLE PHENOMENON IN HIGH SPEED CFD CALCULATIONS

João Henrique A. Azevedo, joaohenrique.azevedo@gmail.com
Instituto Tecnológico de Aeronáutica, São José dos Campos, SP, 12228-900, Brazil

Marcus V. C. Ramalho, mvcramalho@gmail.com
Universidade de Brasília, Brasília, DF, 70919-970, Brazil

João Luiz F. Azevedo, joaoluiz.azevedo@gmail.com
Instituto de Aeronáutica e Espaço, São José dos Campos, SP, 12228-903, Brazil

Abstract. *Some shock-capturing methods can generate spurious solutions when applied to seemingly simple problems such as the calculation of the flowfield containing a detached shock wave ahead of a blunt body in supersonic flow. This numerical problem is known as the carbuncle phenomenon. There is still no universally accepted explanation for the occurrence of the carbuncle phenomenon. The present paper is, therefore, interested in studying the origin of the carbuncle phenomenon. The flowfields of interest to the present work are modeled by the two-dimensional Euler equations. The equations are discretized using a cell-centered-based finite volume procedure, and several well-known numerical flux formulas are used in the spatial discretization of the governing equations. Most test cases addressed in the paper consider the supersonic steady flow around a blunt body. The work advances the possibility that the carbuncle phenomenon could be viewed as some form of a Richtmyer-Meshkov instability. Hence, the authors propose that the origin of the carbuncles is associated with the vorticity generated by the misalignment of pressure gradients across the shock with density gradients artificially created within the non-physical numerical shock structure. Several results that support such possibility are discussed in the paper.*

Keywords: *Carbuncle phenomenon, high speed flow, Euler equations, shock capturing, CFD*

1. INTRODUCTION

It has been known for many years that some shock-capturing methods can generate spurious solutions when applied to seemingly simple problems such as the calculation of the flowfield containing a detached shock wave ahead of a blunt body in supersonic flow. The so-called carbuncle phenomenon, first reported by Peery and Imlay (1988), was initially associated with the use of Roe's approximate Riemann solver (Roe, 1981) in the spatial discretization of the convective terms in the Euler equations. However, it was later found to affect several other methods. In its most typical form, the carbuncle phenomenon consists of a protrusion ahead of the shock, which contains a region of circulating and possibly stagnated flow (Roe *et al.*, 2005; Ramalho and Azevedo, 2010). The overall flowfield appears to satisfy the Euler equations, at least in a weak sense and in its discretized form, since solutions including the carbuncle typically satisfy usual convergence tests. The phenomenon has been observed by several authors, and a fairly extensive literature on its possible causes and cures has been developed (Quirk, 1992; Pandolfi and D'Ambrosio, 2001; Dumbser *et al.*, 2004; Robinet *et al.*, 2000; Chauvat *et al.*, 2005; Roe *et al.*, 2005; Kitamura *et al.*, 2007; Henderson and Menart, 2007).

It has been found that the carbuncle appears to occur only with shock-capturing schemes that are designed to preserve contact discontinuities (Pandolfi and D'Ambrosio, 2001). One explanation is that such schemes provide insufficient dissipation in the shock region, particularly in the direction parallel to the shock (Quirk, 1992; Pandolfi and D'Ambrosio, 2001; Xu, 1999), thereby suffering from instabilities that may result in the formation of the carbuncle. Dumbser *et al.* (2004) analyzed the linear stability of several discretization schemes and concluded that those which are more carbuncle-prone are also likely to be inherently unstable under certain conditions. Quirk (1992) observed that, although adding dissipation in the direction parallel to the shock was a common method to suppress the carbuncle in contact discontinuity-preserving schemes, there were no physical or numerical grounds for resorting to such a "cure". It was simply a convenient means to get rid of the problem.

A different type of explanation was attempted by Robinet *et al.* (2000), who suggested that the origin of the carbuncle could lie in the physical instability of the surface of discontinuity itself, *i.e.*, the shock wave. According to earlier research on the problem of shock wave stability, as described, for example, in Landau and Lifshitz (1959), the plane shock wave formed in a polytropic gas is always stable. Robinet *et al.* (2000), nevertheless, reported to have found a mode which could give rise to instability and that had been overlooked by previous researchers. Moreover, the characteristics of this mode seemed to agree with observations that had been made in connection with the carbuncle phenomenon. This discovery, however, was later contested by Coulombel *et al.* (2002), who reaffirmed that a plane shock wave in a polytropic gas could not, in fact, be physically unstable, and showed that the derivation of Robinet *et al.* (2000) was incorrect in some respects.

As pointed out by Roe *et al.* (2005) and Kitamura *et al.* (2007), we still lack a satisfactory explanation for the occur-

rence of the carbuncle phenomenon. The observation by Xu (1999) that numerical shock instabilities do not occur when unstructured meshes are used in the computation, because the shock would not be systematically aligned with the grid, is not borne out, for instance, by results obtained in the present paper. Kitamura *et al.* (2007) found that the carbuncle may affect schemes which incorporate "entropy corrections" or which provide dissipation of a multidimensional character. As mentioned above, Quirk (1992) noted that there are no physical reasons for the addition of extra doses of dissipation in critical directions in schemes that otherwise correctly preserve contact discontinuities. It seems certain, however, that the carbuncle only occurs in shock-capturing methods, since it has never been observed when a shock-fitting method is used.

On the basis of these observations, previous work by some of the present authors (Ramalho and Azevedo, 2010) proposed that the carbuncle phenomenon may result from a physical instability, namely the Richtmyer-Meshkov instability, whose occurrence is made possible by the fact that the captured shock is not a perfect discontinuity, but rather contains intermediate non-physical states. Such an explanation was motivated by the occurrence of real physical "carbuncles" under certain conditions in experiments with supersonic flows. It should be emphasized that the proposed rationale differs from the suggestion of Robinet *et al.* (2000), referred to above, in that the physical instability involved in the present hypothesis is not that of the sharp and discontinuous shock wave itself, but, as will be explained later, that of the interaction between a shock wave and density inhomogeneities. Further work by the present authors (Ramalho *et al.*, 2011) also demonstrated that, if there is no numerical shock structure, for instance, when a shock-fitting method is used, then there is no carbuncle regardless of the spatial discretization scheme used.

2. GOVERNING EQUATIONS AND NUMERICAL PROCEDURE

The flow is modeled by the two-dimensional Euler equations, which can be written in integral form as

$$\frac{\partial}{\partial t} \int_V Q \, dV + \int_S (E \, \mathbf{i} + F \, \mathbf{j}) \cdot \mathbf{n} \, dS = 0 \,, \tag{1}$$

where V denotes a control volume, S represents its boundary and $\mathbf{n}$ is the outward normal to the S boundary. The vector of conserved quantities, Q, and the convective flux vectors, E and F, are given by

$$\begin{aligned}
Q &= \begin{bmatrix} \rho, & \rho u, & \rho v, & e \end{bmatrix}^T \,, \\
E &= \begin{bmatrix} \rho u, & \rho u^2 + p, & \rho uv, & (e + p) \, u \end{bmatrix}^T \,, \\
F &= \begin{bmatrix} \rho v, & \rho uv, & \rho v^2 + p, & (e + p) \, v \end{bmatrix}^T \,.
\end{aligned} \tag{2}$$

In these definitions, ρ denotes the density, p is the pressure, u and v represent the Cartesian velocity components, and e is the total energy per unit volume.

The equations are discretized using a cell-centered based finite volume procedure, where the discrete vector of conserved variables, Q_i, is defined as an average over the i-th control volume as

$$Q_i = \frac{1}{V_i} \int_{V_i} Q \, dV \,. \tag{3}$$

With this definition, Eq. (1) can be rewritten for the i-th control volume as

$$\frac{d}{dt} (V_i \, Q_i) + \int_{S_i} (E \, dy - F \, dx) = 0 \,. \tag{4}$$

In the spatial discretization, the surface integral in Eq. (4) is approximated by

$$C (Q_i) = \sum_{k=1}^{n} [E (Q_{ik}) \, \Delta y_{ik} - F (Q_{ik}) \, \Delta x_{ik}] \,, \tag{5}$$

where k spans the n control volumes which are neighbors of the i-th volume, $E_{ik} = E (Q_{ik})$ and $F_{ik} = F (Q_{ik})$ are the numerical convective fluxes between the i and k volumes, and the Δx_{ik} and Δy_{ik} terms are calculated as

$$\Delta x_{ik} = x_{k_2} - x_{k_1} \qquad \text{and} \qquad \Delta y_{ik} = y_{k_2} - y_{k_1} \,, \tag{6}$$

where the points (x_{k_1}, y_{k_1}) and (x_{k_2}, y_{k_2}) are the vertices which define the interface between the i and k cells.

The spatial discretization thus consists in *(i)* determining the geometry of the control volumes or cells (in other words, choosing a mesh); and *(ii)* determining the intercell (or numerical) fluxes, E_{ik} and F_{ik}, by means of an appropriate scheme. In the present paper, unstructured triangular and quadrilateral meshes are employed, and the intercell numerical fluxes are calculated using different numerical flux functions. In particular, the results included in the paper have used Liou's first-order AUSM$^+$ scheme (Liou, 1996), Jameson's centered scheme (Jameson *et al.*, 1981), van Leer's flux-vector splitting first-order method (van Leer, 1996), Roe's original scheme (Roe, 1981) and a weighted essentially nonoscillatory

(WENO) scheme (Wolf and Azevedo, 2006, 2007) constructed using Roe's approximate Riemann solver. The approach adopted in the present work to extend the formulation of the first four methods to unstructured meshes follows Azevedo and Korzenowski (1998) and Figueira da Silva *et al.* (2000), and it consists in defining a local one-dimensional system normal to the interface considered. Once the convective operator, $C(Q_i)$, is calculated, Eq. (4) can be advanced in time. In the present simulations, a fully explicit, 5-stage, Runge-Kutta method is used as the time-stepping scheme (Azevedo and Korzenowski, 1998; Figueira da Silva *et al.*, 2000).

3. THE BASIC TEST CASE

The basic test case considered in the present work and that, actually, motivated the present research is the calculation of the two-dimensional, supersonic, inviscid flow of a polytropic gas ($\gamma = 1.4$) around a cylinder at zero angle of attack. Several different meshes have been used in the present investigation and a detailed account of these mesh topologies and refinement levels are discussed together with each study here described. In particular, the geometry of the problem together with an unstructured triangular mesh are shown in Fig. 1. The previously described finite volume code is used in all computations (Figueira da Silva *et al.*, 2000; Wolf and Azevedo, 2006, 2007). As already discussed, the code has implemented several different spatial discretization schemes, and the effects of each particular spatial discretization scheme are discussed in the forthcoming sections.

(a)   (b)
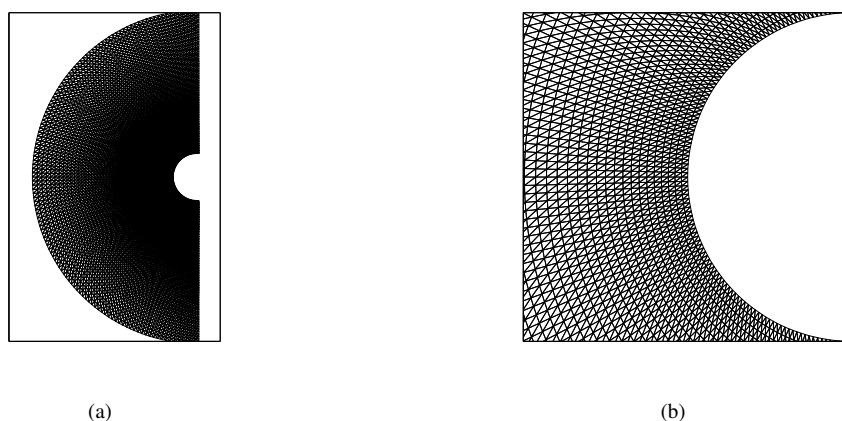
Figure 1. Basic test case: a) Computational domain, mesh and cylinder; b) Detail of a typical triangular mesh.

Uniform freestream flow conditions are initially prescribed throughout the entire domain. As to boundary conditions, freestream properties are imposed along the far field boundary, *i.e.*, the left part of the computational domain in Fig. 1(a), and slip conditions are enforced on the cylinder surface. Zero-order extrapolation of all properties is employed on downstream boundaries, *i.e.*, the right limits of the domain in Fig. 1(a). Figure 2(a) shows Mach number contours for a freestream Mach number (M_∞) of 12.2. This particular calculation was performed using a 1st-order accurate spatial discretization based on Liou's AUSM$^+$ method (Liou, 1996). The carbuncle is clearly visible above the symmetry line, between the shock and the cylinder. It must be noted that the mesh itself is not symmetric. Figure 2(b) displays a detailed view of the carbuncle and shows velocity vectors forming a vortex-like pattern around a region of nearly stagnated flow. Figure 2(c) shows the evolution of the L_2 norm of the density residue and confirms that it decreases by more than ten orders of magnitude, thereby attesting to the numerical convergence of the solution. It must be emphasized that the computations that led to the results in Fig. 2 were run in steady state mode, *i.e.*, these calculations were run assuming a constant CFL number throughout the flowfield.

4. BAROCLINIC VORTICITY GENERATION

It was noted by Roe (2001) and by Roe *et al.* (2005) that numerically generated carbuncles resemble flows that may be physically realized by the introduction of plates or spikes in front of a blunt body immersed in supersonic flow. However, flow structures that resemble carbuncles can also be created by the interaction between axial vortices and shock waves. For instance, Kalkhoran *et al.* (1991, 1998) and Cattafesta and Settles (1992) set up experiments in which tip axial vortices generated by a wedge impinged on detached shock waves formed in front of blunt bodies in supersonic flow. It is observed that, as a result of this interaction, the shock wave bulged forward in the upstream direction or acquired a conical shape, behind which a highly unsteady flow pattern develops. Similarly, Thomer *et al.* (2001) conducted numerical simulations of the interaction of a plane shock with an axial vortex. Illustrations of the flows that result from such interactions can be seen in the original cited references or in Ramalho and Azevedo (2010). For all of these cases, the flow patterns that are

(a) Mach number contours

(b) Detail of velocity vectors

(c) Convergence history
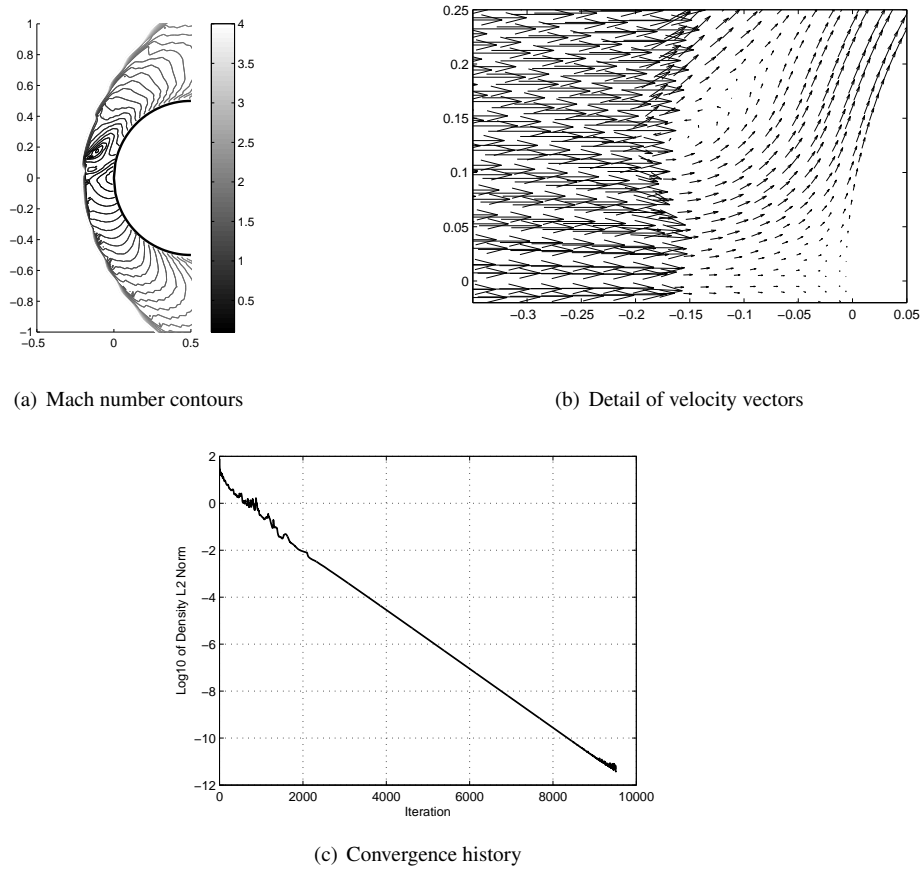
Figure 2. Computation with a carbuncle, $M_\infty = 12.2$. Numerical scheme is AUSM$^+$.

developed, although related to physical phenomena, could well be recognized as the carbuncles which are common in the CFD literature.

In the context of the investigation of shock waves formed within plasmas, Kremeyer *et al.* (2002) sought to demonstrate that the phenomenon of "shock splitting" observed in some experiments should not be attributed to electromagnetic effects, but rather to the purely gas dynamic effect of the shock, which can curve and bow as it passes through transverse density (or temperature) profiles. In this connection, those authors observed that vorticity is generated at the shock by means of the so-called *baroclinic* mechanism. This corresponds to a source term in the vorticity evolution equation which has the following form:

$$\left(\frac{\partial \omega}{\partial t} \right)_B = \text{grad}\,(\rho) \times \text{grad}\,(p) \,/\, \rho^2 \,. \tag{7}$$

Such observation has prompted the present authors to reproduce this phenomenon of shock bowing in the simulation of the basic test case described in Section 3. It should also be noted that the transverse density gradients used to deform the shock in the simulations of Kremeyer *et al.* (2002) are also present in the interactions of the shock with axial vortices investigated in Kalkhoran *et al.* (1991), Kalkhoran *et al.* (1998), Cattafesta and Settles (1992) and Thomer *et al.* (2001). The density profiles of the axial vortices simulated by Thomer *et al.* (2001), in particular, have a form similar to the one used in the present work.

5. THE RICHTMYER-MESHKOV INSTABILITY

In 1960, Richtmyer (1960) presented the linear stability analysis of a plane surface subject to a small sinusoidal perturbation accelerated by a shock. He found that such a configuration would be unstable and his prediction was later confirmed in experiments reported by Meshkov (1970). This phenomenon, which more generally involves the interaction of shock waves with density inhomogeneities (Samtaney *et al.*, 1998), came to be known as the "Richtmyer-Meshkov instability." The deposition of circulation is the dominant fluid dynamical process in the early stages of the development of the Richtmyer-Meshkov instability (Samtaney *et al.*, 1998). As a moving shock traverses an interface, a misalignment

of pressure and density gradients leads to rapid vorticity deposition on the interface by means of the baroclinic mechanism indicated in Eq. (7). This may occur not only with an interface which is made non-planar because of a perturbation, but also in the case of a planar interface initially at an angle with the shock.

The problem investigated in Samtaney *et al.* (1998) is the physical Richtmyer-Meshkov instability that arises as the shock crosses the oblique interface. However, the same environment that is set up just prior to the physical occurrence of the Richtmyer-Meshkov instability can be realized on a smaller scale as a result of the spatial discretization of the flowfield, with the assumption of uniform, averaged flow properties within each cell, and the application of a shock-capturing method, which produces intermediate states within the numerical shock. If the cells and their interfaces could be regarded as physical regions of gas at different states separated by physical interfaces, then the portions of the numerical grid, where pressure and density gradients are of such magnitude and direction as to produce strong vorticity deposition via the baroclinic mechanism, could be susceptible to instability in roughly the same way as the physical configuration discussed in Samtaney *et al.* (1998) is susceptible to the Richtmyer-Meshkov instability.

This observation motivated the definition of a parameter based on Eq. (7) which seeks to measure the intensity of baroclinic vorticity generation within, and immediately upstream of, the numerical shock (Ramalho and Azevedo, 2010). As the flow solver advances the computation in time, the maximum value of this parameter throughout the flow field is calculated according to the following algorithm:

1. At each iteration, find the cells in which the density is larger than the freestream density, using some practical threshold value, *e.g.*, $\rho \geq 1.01\,\rho_\infty$, and which have at least one neighbor cell whose density is approximately equal to or smaller than that of the undisturbed flowfield, *e.g.*, $\rho \leq 1.01\,\rho_\infty$. These cells, which will be named "0-cells," should correspond to "intermediate" states created by the shock-capturing method. Store the pressure and density of these cells as p_0 and ρ_0, respectively;

2. For each 0-cell found in (1), identify the neighbor cell for which the pressure is largest among the neighbors. Call this neighbor a "1-cell". Store its pressure as p_1;

3. For each 0-cell found in (1), identify the neighbor whose density is approximately equal to that of the undisturbed flow field. Call this neighbor a "b-cell". Store its density as ρ_b;

4. For each 0-cell found in (1), find the angle between the normal direction to the interface between the 0-cell and the 1-cell and the normal direction to the interface between the 0-cell and the b-cell. Call this angle θ;

5. For each 0-cell found in (1), calculate the quantity

$$k = |p_1 - p_0| * |\rho_b - \rho_0| * |\sin\theta| / \rho_0^2 ; \tag{8}$$

6. Identify the 0-cell where k is a maximum at the given iteration. Store the value of k and the position of this 0-cell. Advance the solution to the next time step and return to (1).

This algorithm was successfully applied to some numerical tests in Ramalho and Azevedo (2010) and some additional tests are reported in the forthcoming sections. As one can see from the cited reference and the discussion in the present paper, the location of the points where the k parameter attains its largest values, as well as the magnitude of the parameter, seem to correlate with the occurrence, or the absence, of carbuncles in the computational tests.

6. RESULTS AND DISCUSSION

The first aspect addressed concerns the generation of carbuncles by imposing a transverse density gradient upstream of the shock and, hence, numerically generating carbuncles that resemble the ones obtained in the experimental results discussed in Section 4. Hence, the idea is that the superposition of a narrow region containing a transverse density gradient upstream of the shock, obtained in the two-dimensional calculation described in Section 3, should make the shock bulge forward as the calculation is further advanced in time, at least during some transient period. Moreover, the numerical experiment considered both the spatial discretization with the AUSM$^+$ scheme (Liou, 1996) and with a centered scheme (Jameson *et al.*, 1981). The latter is a central difference-type scheme in which artificial dissipation is explicitly provided, and such a scheme is not particularly suited for the calculation of hypersonic flows but, on the other hand, it is not prone to the appearance of carbuncles.

Velocity vector plots are shown in Fig. 3 for the converged solutions obtained with the AUSM$^+$ scheme and with the centered scheme, for simulations performed as described in Section 3. These particular calculations were preformed in steady state mode, that is, the time march of the equations considers a constant CFL number. Moreover, both calculations formally converge, *i.e.*, the residues go to machine zero. For instance, the velocity vectors shown in Fig. 3(a) correspond to the same simulation whose results are shown in Fig. 2. As one can clearly see in Fig. 2(c), there is formal residue convergence. Furthermore, as expected, the solution with the AUSM$^+$ scheme exhibits a carbuncle whereas the one

(a) AUSM$^+$

(b) Centered scheme
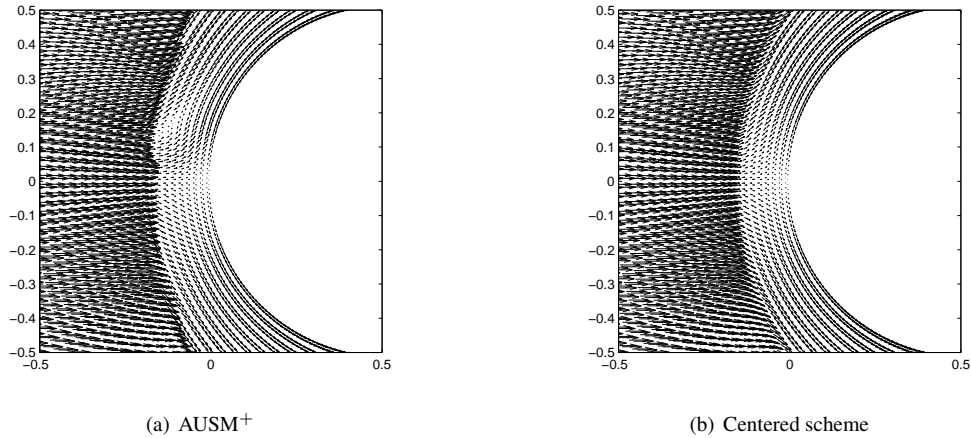
Figure 3. Converged shock solutions (velocity vectors) for blunt body with $M_\infty = 12.2$.
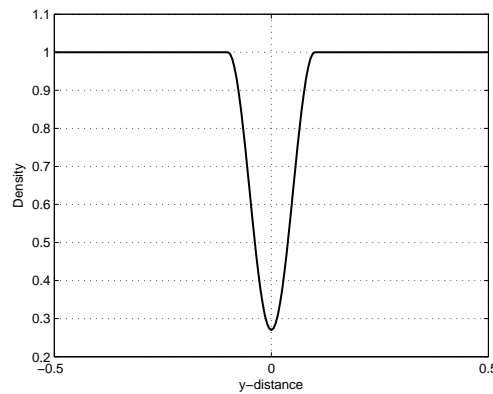
Figure 4. Upstream density profile associated with axial vortices. This profile is used in the simulations that led to the results shown in Fig. 5.

with the centered scheme does not. The next step was to superimpose on these converged solutions, upstream of the obtained shocks, a density gradient and, then, to restart the calculation for a few more iterations. The density gradient profile used is shown in Fig. 4. Figure 5, then, presents detailed views of the velocity vectors in the region near the shock protrusion generated by the interaction of the shock with the transverse density gradient after 100 iterations of the restarted calculation. The very strong carbuncle-like behavior is clearly evident in both plots in Fig. 5. Moreover, one can also see that the original recirculation region is still present in the results obtained with the AUSM$^+$ scheme (see Fig. 5(a)). However, if one allows the calculation to progress, this original "carbuncle" will eventually disappear, at least for the present test case. Furthermore, it is important to emphasize that a deformed shock was obtained not only with the use of the AUSM$^+$ method, but also with a central difference-type scheme in which artificial dissipation is explicitly provided.

On the basis of these results and other test cases discussed in Ramalho and Azevedo (2010), it appears to be possible that carbuncles may be "physically" created via the baroclinic mechanism of vorticity generation, where strong pressure gradients induced by the shock interact with some transverse density gradients. In the experiments discussed in Section 4 and in the above results, the transverse density gradient is externally provided, either artificially or by means of axial vortices impinging on the shock. The aspect that the authors are interested in understanding is precisely the source of such "spurious" baroclinic interaction in the calculation of the flow by a shock-capturing method. Since carbuncles have never been found when a shock-fitting procedure is used, it seems that a possible source of the instability associated with the carbuncle could be found by investigating whether the intermediate non-physical states generated by shock-capturing schemes have the potential of inducing baroclinic vorticity generation, particularly in the transient stages of the calculation.

Another set of tests conducted in the present work addressed the effects of the spatial discretization schemes. Hence, besides the AUSM$^+$ and centered schemes, other spatial discretization schemes have been used as previously discussed. For instance, the same basic test case was also run using a 2nd-order WENO scheme (Wolf and Azevedo, 2006, 2007), constructed using the Roe scheme for its numerical flux function, and with the same unstructured triangular mesh shown in Fig. 1. The results are shown in Fig. 6, which presents both Mach number and dimensionless density contours superimposed on flow streamlines, for the relevant region upstream of the blunt body. The carbuncle is again clearly visible in

(a) AUSM$^+$

(b) Centered scheme
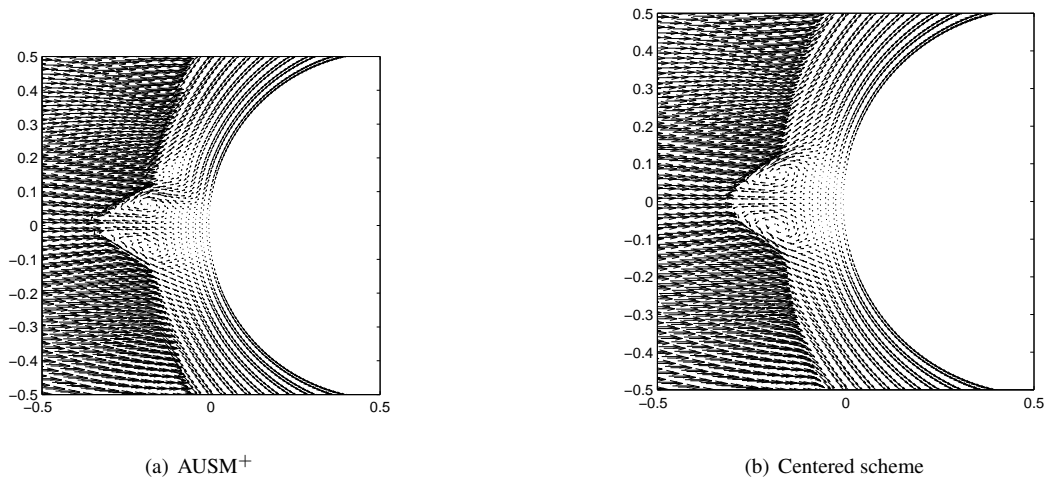
Figure 5. Velocity vectors at iteration 100, starting with upstream transverse density gradient superimposed to previous converged shock solutions, $M_\infty = 12.2$.

these figures, as well as the slight protusion of the shock due to the presence of the recirculation region just downstream of it. The results in Fig. 6 also represent a fully converged steady state solution. For the several calculations performed,

(a) Mach number contours.

(b) Dimensionless density contours.
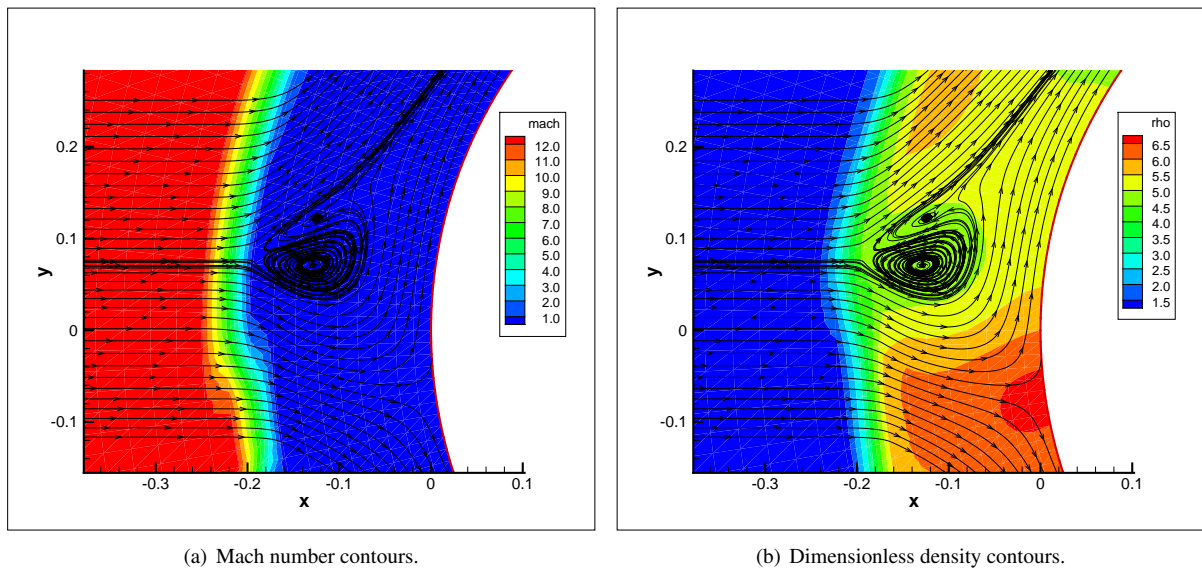
Figure 6. Inviscid calculation of the blunt body flow for $M_\infty = 12.2$ with a 2nd-order WENO scheme. Streamlines superimposed to property contours.

simulations with the centered scheme (Jameson *et al.*, 1981) and simulations with the 1st-order van Leer scheme (van Leer, 1996) did not yield carbuncles, regardless of the mesh used. On the other hand, all calculations that used AUSM$^+$ (Liou, 1996) or the Roe scheme (Roe, 1981) as their basic numerical flux function have yielded results with carbuncles. In that regard, as already shown, the WENO scheme (Wolf and Azevedo, 2006), built using the Roe approximate Riemann solver, has also resulted in carbuncles. The use of constant CFL or constant time step in the numerical integration does not change the characteristics of the result, as far as the appearance of carbuncles in the flow is concerned.

All of the computations described so far have assumed a constant CFL number and, therefore, one was clearly seeking a steady state solution. It was observed, however, that some calculations, specially with finer grids and using higher order methods, do not yield steady results. In particular, in the present case, computations have been performed with 2nd- and 3rd-order WENO schemes (Wolf and Azevedo, 2006) and, for some cases, typically with finer grids, the results were unsteady. Hence, computations have also been performed for a constant time step throughout the flowfield, such that the resulting computational transient could have some physical meaning, despite the impulsive start initial condition. It has been observed that, after the detached shock wave establishes itself, and regardless of whether the solution converges to a steady state or not, carbuncles are clearly generated at the shock. They grow in size and are, eventually, shed and

(a) $t = 0.0128$

(b) $t = 0.0684$

(c) $t = 0.0836$

(d) $t = 0.1200$
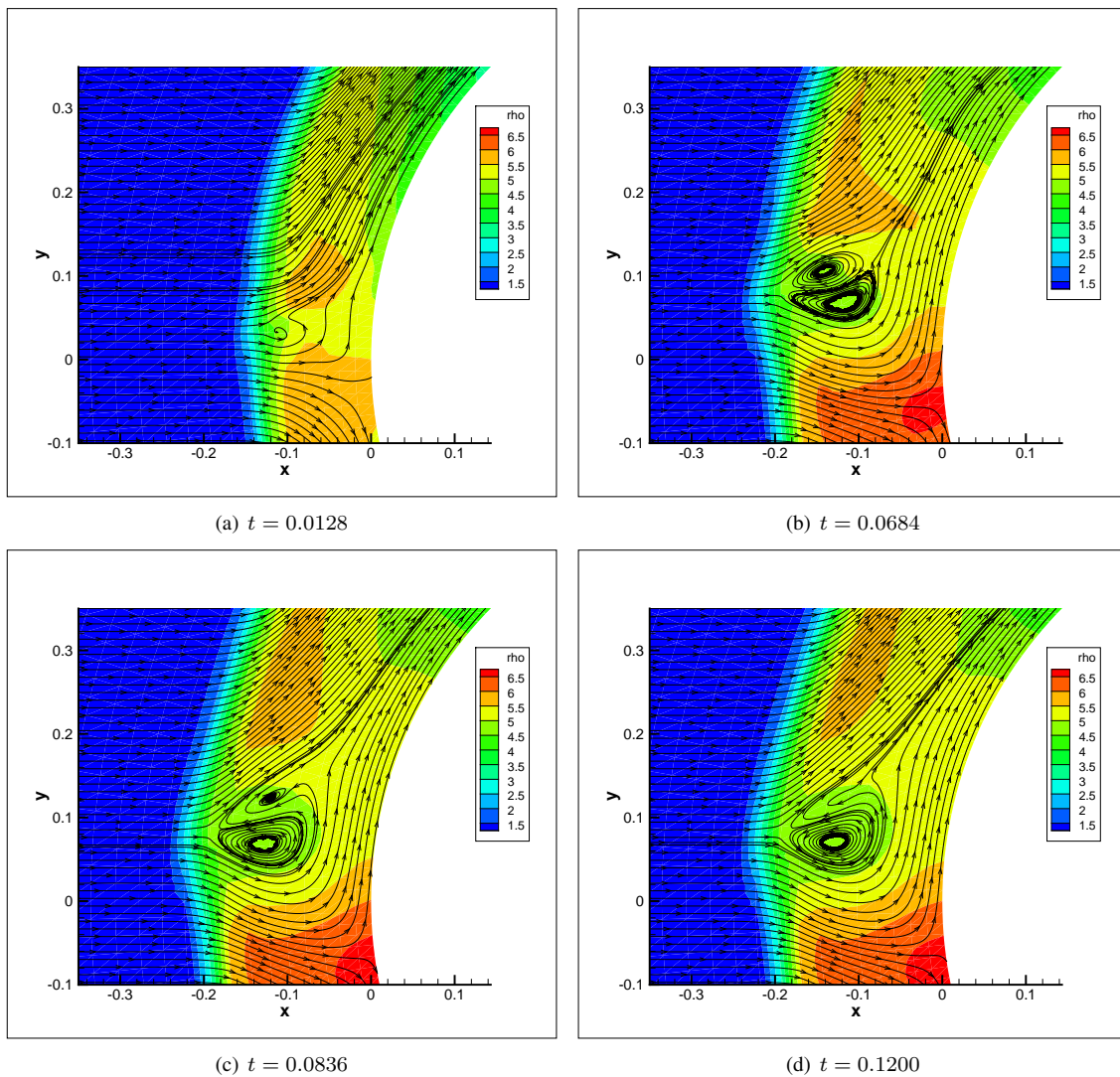
Figure 7. Inviscid calculation of the blunt body flow for $M_\infty = 12.2$ with a 2nd-order WENO scheme. Instantaneous particle paths are superimposed to density contours and time is reported in dimensionless units after the impulsive start of the computation.

convected by the flow. For most calculations, however, this process converges to a steady state solution with a carbuncle immediately downstream of the shock, independently of the simulation being run with a constant CFL or a constant time step. Further visualization of this convergence process can be seen in Fig. 7, which shows calculations with the same 2nd-order WENO scheme previously discussed. The difference is that, in this case, the simulation is run with a constant time step. The figure shows four snapshots of the flow solution for the same basic test case, visualized in terms of density contours superimposed to instantaneous particle paths. Actually, in this case, the particle paths will become streamlines, because the solution does converge to steady state. However, the authors are not calling them streamlines yet in the figure, because these are still snapshots of an unsteady calculation, which is evolving to a converged solution. One can clearly see that the instantaneous flow visualization shown in Fig. 7(c) seems actually more similar to the final converged solution, shown in Fig. 6, than the result in Fig. 7(d). However, as already mentioned, carbuncles are created at the shock, grow in size and are convected by the flow, except that, in this particular simulation, the solution converges to a steady flow configuration.

The final aspect addressed in the present work concerns the test of the parameter, defined in Section 5, that attempts to measure the intensity of baroclinic vorticity generation in the numerical shock. Ramalho and Azevedo (2010) have run several tests with this, so-called, k parameter, including tests for a supersonic blunt body flow, as the test case used in the present paper, and tests for a planar shock wave propagating down in a duct. Further investigation of the use of the k parameter to correlate the occurrence of maximum values of spurious vorticity generation in the numerical shock structure and the initial appearance of carbuncles is also reported in Ramalho *et al.* (2011). The results ran in the context of the present work further support the conclusion that there is a strong correlation between the spurious vorticity generation

in the shock wave via the baroclinic mechanism, as measured by the k parameter, and the occurrence of carbuncles in the numerical solution. Furthermore, the simulations have shown that some methods have a tendency of generating very large values of k, whereas others yield very low levels of k for the same problem and, even, the same computational grid. The former methods have carbuncles, whereas the latter do not. In the interest of brevity, the main observations from the simulations which attempt to verify how the k parameter could be related to carbuncle appearance can be summarized as follows.

1. If one plots the maximum value of the k parameter over the flowfield as the iterations proceed, it becomes clear that the maximum value of the k parameter over the flowfield attains a series of peaks as the calculation evolves from the initial freestream flow imposed over the entire domain to a shock wave that detaches itself away from the surface of the cylinder.

2. The geometric location of the cells where k attains such peak values, as the computation evolves over time, correlates with the trace of the spatial positions in the flowfield where carbuncles are being formed as the solution converges.

3. The overall highest value of the k parameter throughout the simulation correlates with both the location where a negative velocity component in the freestream direction first appears, for the blunt body flow simulation, and the instant of time, along the simulation, in which such a situation occurs. It must be observed that the first occurrence of a negative velocity component in the freestream direction, for the present test case, gives an indication of the first stage in the development of a vortex characteristic for the carbuncles.

4. Spatial discretization schemes, which are prone to yield solutions with carbuncles, typically have fairly large values of maximum k at the shock wave throughout the calculation process. On the other hand, schemes which are known not to produce carbuncles have much lower values of maximum k throughout the history of the simulation.

7. A SHOCK-FITTING PROCEDURE

Although the evidence provided by all the tests previously discussed seemed quite compelling, another form of looking at the problem was envisioned in order to further demonstrate the present proposal. Since the origin of the problem seems to be associated to the nonphysical states which necessarily appear within the numerical shock structure, previous work (Ramalho *et al.*, 2011) has considered an additional test for such hypothesis. A shock-fitting procedure (Salas, 2010) for steady flow was developed for the unstructured conservative finite volume code described in Section 2. The objective was to verify whether carbuncles develop in the flowfield if the same code is run in a shock-fitting mode. If no carbuncles appear, this would support the proposal emphasized in the present work. Further details on shock-fitting methods and, in particular, on the concept of the "floating" shock-fitting method for unstructured meshes can be seen in Salas (2010) and Paciorri and Bonfiglioli (2010). A detailed account of the procedure implemented by the present authors is described in Ramalho *et al.* (2011). The results in this last reference clearly indicate that no carbuncles appear when the code is run in shock-fitting mode, regardless of the spatial discretization scheme used. Therefore, the authors believe that such results lend further support to the proposal of the present paper.

8. CONCLUDING REMARKS

The paper presents an investigation of a possible explanation for the generation of "carbuncles" in high speed flow solutions calculated by some shock-capturing schemes. The main argument put forward in the paper is that, by introducing nonphysical states in the solution, shock-capturing schemes could create the conditions for the development of an instability that is physically and inherently related to the interaction of shock waves with density inhomogeneities, the so-called Richtmyer-Meshkov instability. Several simulations of 2-D inviscid flows over a blunt body have been obtained and these calculations considered a wide variety of numerical spatial discretization schemes. Some of these computations were run in steady state mode, *i.e.*, using a constant CFL number throughout the flowfield, whereas others considered a constant time step. All simulations indicated that carbuncles are formed at the detached shock wave. Moreover, all simulations corroborate the present proposal, that is, that the origin of the carbuncle phenomenon seems to be associated with density and pressure gradient misalignments due to the nonphysical states which appear within the numerical shock structure. Furthermore, previous calculations, in which a shock-fitting procedure has been coupled to the present code, demonstrate that no carbuncles appear when the code is run in shock-fitting mode. Hence, in summary, it seems that there is some very compelling evidence that carbuncles originate due to a Richtmyer-Meshkov-type instability, owing to the interaction between shock waves and density inhomogeneities, which are created within the nonphysical structure of numerical shock waves in shock-capturing schemes.

9. ACKNOWLEDGMENTS

10. REFERENCES

Azevedo, J.L.F. and Korzenowski, H., 1998. "Comparison of unstructured grid finite volume methods for cold gas hypersonic flow simulations". In *16th AIAA Applied Aerodynamics Conference*. AIAA Paper No. 98-2629, Albuquerque, NM.

Cattafesta, L.N. and Settles, G.S., 1992. "Experiments on shock-vortex interactions". In *30th AIAA Aerospace Sciences Meeting and Exhibit*. AIAA Paper No. 92-0315, Reno, NV.

Chauvat, Y., Moschetta, J.M. and Gressier, J., 2005. "Shock wave numerical structure and the carbuncle phenomenon". *International Journal for Numerical Methods in Fluids*, Vol. 47, No. 8-9, pp. 903–909.

Coulombel, J.F., Benzoni-Gavage, S. and Serre, D., 2002. "Note on a paper by Robinet, Gressier, Casalis and Moschetta". *Journal of Fluid Mechanics*, Vol. 469, pp. 401–405.

Dumbser, M., Moschetta, J.M. and Gressier, J., 2004. "A matrix stability analysis of the carbuncle phenomenon". *Journal of Computational Physics*, Vol. 197, No. 2, pp. 647–670.

Figueira da Silva, L.F., Azevedo, J.L.F. and Korzenowski, H., 2000. "Unstructured adaptive grid flow simulations of inert and reactive gas mixtures". *Journal of Computational Physics*, Vol. 160, No. 2, pp. 522–540.

Henderson, S. and Menart, J., 2007. "Grid study on blunt bodies with the carbuncle phenomenon". In *39th AIAA Thermophysics Conference*. AIAA Paper No. 2007-3904, Miami, FL.

Jameson, A., Schmidt, W. and Turkel, E., 1981. "Numerical solution of the Euler equations by finite volume methods using Runge-Kutta time-stepping schemes". In *14th AIAA Fluid and Plasma Dynamics Conference*. AIAA Paper No. 81-1259, Palo Alto, CA.

Kalkhoran, I.M., Sforza, P.M. and Wang, F.Y., 1991. "Experimental study of shock-vortex interaction in a Mach 3 stream". In *15th AIAA Computational Fluid Dynamics Conference*. AIAA Paper No. 91-3270.

Kalkhoran, I.M., Smart, M.K. and Wang, F.Y., 1998. "Supersonic vortex breakdown during vortex/cylinder interaction". *Journal of Fluid Mechanics*, Vol. 369, pp. 351–380.

Kitamura, K., Roe, P. and Ismail, F., 2007. "An evaluation of Euler fluxes for hypersonic flow computations". In *18th AIAA Computational Fluid Dynamics Conference*. AIAA Paper No. 2007-4465, Miami, FL.

Kremeyer, K., Nazarenko, S. and Newell, A.C., 2002. "Shock bowing and vorticity dynamics during propagation into different transverse density profiles". *Physica D*, Vol. 163, No. 3-4, pp. 150–165.

Landau, L.D. and Lifshitz, E.M., 1959. *Fluid Mechanics*. Pergamon Press, New York.

Liou, M.S., 1996. "A sequel to AUSM: AUSM$^+$". *Journal of Computational Physics*, Vol. 129, No. 2, pp. 364–382.

Meshkov, Y.Y., 1970. "Instability of a shock wave accelerated interface between two gases". NASA TT F-13074, NASA Technical Translation.

Paciorri, R. and Bonfiglioli, A., 2010. "An unstructured shock-fitting solver for two-dimensional flows". Retrieved at <http://www.difa.unibas.it/utenti/bonfiglioli/pub/aimeta07.pdf>.

Pandolfi, M. and D'Ambrosio, D., 2001. "Numerical instabilities in upwind methods, analysis and cures for the carbuncle phenomenon". *Journal of Computational Physics*, Vol. 166, No. 2, pp. 271–301.

Peery, K.M. and Imlay, S.T., 1988. "Blunt body flow simulations". In *24th AIAA/ASME/SAE/ASEE Joint Propulsion Conference*. AIAA Paper No. 88-2904, Boston, MA.

Quirk, J.J., 1992. "A contribution to the great Riemann solver debate". ICASE Report No. 92-64, ICASE.

Ramalho, M.V.C., Azevedo, J.H.A. and Azevedo, J.L.F., 2011. "Further investigation into the origin of the carbuncle phenomenon in aerodynamic simulations". In *49th AIAA Aerospace Sciences Meeting Including the New Horizons Forum and Aerospace Exposition*. AIAA Paper No. 2011-1184, Orlando, FL.

Ramalho, M.V.C. and Azevedo, J.L.F., 2010. "A possible mechanism for the appearance of the carbuncle phenomenon in aerodynamic simulations". In *48th AIAA Aerospace Sciences Meeting Including the New Horizons Forum and Aerospace Exposition*. AIAA Paper No. 2010-0872, Orlando, FL.

Richtmyer, R.D., 1960. "Taylor instability in shock acceleration of compressible fluids". *Communications on Pure and Applied Mathematics*, Vol. 13, No. 2, pp. 297–319.

Robinet, J.C., Gressier, J., Casalis, G. and Moschetta, J.M., 2000. "Shock wave instability and carbuncle phenomenon: Same intrinsic origin?" *Journal of Fluid Mechanics*, Vol. 417, pp. 237–263.

Roe, P., 2001. "Vorticity capturing". In *15th AIAA Computational Fluid Dynamics Conference*. AIAA Paper No. 2001-2523, Anaheim, CA.

Roe, P., Nishikawa, H., Ismail, F. and Scalabrin, L.C., 2005. "On carbuncles and other excrescences". In *17th AIAA*

Computational Fluid Dynamics Conference. AIAA Paper No. 2005-4872, Toronto, Canada.

Roe, P.L., 1981. "Approximate Riemann solvers, parameter vectors, and difference schemes". *Journal of Computational Physics*, Vol. 43, No. 2, pp. 357–372.

Salas, M.D., 2010. *A Shock-Fitting Primer*. CRC Press, New York.

Samtaney, R., Ray, J. and Zabusky, N.J., 1998. "Baroclinic circulation generation on shock accelerated slow/fast gas interfaces". *Physics of Fluids*, Vol. 10, No. 5, pp. 1217–1230.

Thomer, O., Schröder, W. and Krause, E., 2001. "Normal shock vortex interaction". RTO MP-069(I).

van Leer, B., 1996. "Flux-vector splitting for the Euler equations". *Lecture Notes in Physics*, Vol. 170, pp. 364–382.

Wolf, W.R. and Azevedo, J.L.F., 2006. "High-order unstructured essentially nonoscillatory and weighted essentially nonoscillatory schemes for aerodynamic flows". *AIAA Journal*, Vol. 44, No. 10, pp. 2295–2310.

Wolf, W.R. and Azevedo, J.L.F., 2007. "High-order ENO and WENO schemes for unstructured grids". *Int. J. Numer. Meth. Fluids*, Vol. 55, No. 10, pp. 917–943.

Xu, K., 1999. "Gas evolution dynamics in Godunov-type schemes and analysis of numerical shock instability". ICASE Paper, ICASE.

11. Responsibility notice

The authors are the only responsible for the printed material included in this paper.